

On the Multi-Reference Nature of Plutonium Oxides: PuO_2^{2+} , PuO_2 , PuO_3 and $\text{PuO}_2(\text{OH})_2$

Katharina Boguslawski*

*Institute of Physics, Faculty of Physics, Astronomy and Informatics,
Nicolaus Copernicus University in Torun, Grudziadzka 5, 87-100 Torun, Poland*

Florent Réal, André Severo Pereira Gomes, and Valérie Vallet†

Univ. Lille, CNRS, UMR 8523 - PhLAM - Physique des Lasers Atomes et Molécules, F-59000 Lille, France

Paweł Tecmer‡

*Institute of Physics, Faculty of Physics, Astronomy and Informatics,
Nicolaus Copernicus University in Torun, Grudziadzka 5, 87-100 Torun, Poland*

Corinne Duperrouzel

*Univ. Lille, CNRS, UMR 8523 - PhLAM - Physique des Lasers Atomes et Molécules, F-59000 Lille, France and
Department of Chemistry and Chemical Biology, McMaster University,
Hamilton, 1280 Main Street West, L8S 4M1, Canada*

Örs Legeza

*Strongly Correlated Systems “Lendület” Research Group,
Wigner Research Center for Physics, H-1525 Budapest, Hungary*

Paul W. Ayers

*Department of Chemistry and Chemical Biology, McMaster University,
Hamilton, 1280 Main Street West, L8S 4M1, Canada*

Actinide-containing complexes present formidable challenges for electronic structure methods due to the large number of degenerate or quasi-degenerate electronic states arising from partially occupied 5f and 6d shells. Conventional multi-reference methods can treat active spaces that are often at the upper limit of what is required for a proper treatment of species with complex electronic structures, leaving no room for verifying their suitability. In this work we address the issue of properly defining the active spaces in such calculations, and introduce a protocol to determine optimal active spaces based on the use of the Density Matrix Renormalization Group algorithm and concepts of quantum information theory. We apply the protocol to elucidate the electronic structure and bonding mechanism of volatile plutonium oxides (PuO_3 and $\text{PuO}_2(\text{OH})_2$), species associated with nuclear safety issues for which little is known about the electronic structure and energetics. We show how, within a scalar relativistic framework, orbital-pair correlations can be used to guide the definition of optimal active spaces which provide an accurate description of static/non-dynamic electron correlation, as well as to analyse the chemical bonding beyond a simple orbital model. From this bonding analysis we are able to show that the addition of oxo- or hydroxo-groups to the plutonium dioxide species considerably changes the pi-bonding mechanism with respect to the bare triatomics, resulting in *bent* structures with considerable multi-reference character.

I. INTRODUCTION

Plutonium oxides are ubiquitous in the nuclear industry, either as components of nuclear fuels or of fission products[1, 2]. Due to its extreme radio toxicity, the consequences of an eventual release of plutonium to the environment in the event of nuclear (such as in the Fukushima Daiichi plant, where one reactor was loaded with mixed uranium and plutonium oxide (MOX) fuels) or industrial accidents (like a solvent fire in a facility performing the

PUREX [3, 4] process for reprocessing of spent nuclear fuel) would be severe.

In preparing for such eventualities it is essential to be able to predict the most likely state of the metal, what kind of chemical reactions can potentially occur, and the effect of these in the dispersion of these species outside the containment vessels etc. It is known, for instance, that in the presence of steam and oxygen, plutonium is released primarily as $\text{PuO}_3(\text{g})$ and $\text{PuO}_2(\text{OH})_2(\text{g})$, and less probably as $\text{PuO}_2(\text{g})$ [5], meaning that these could be a potentially important source of radioactive aerosols and transported over long distances.

The considerable difficulties in performing systematic experiments with these materials mean that the reactivity of plutonium and other extremely radioactive species

* k.boguslawski@fizyka.umk.pl

† valerie.vallet@univ-lille1.fr

‡ ptecmer@fizyka.umk.pl

is still not very well understood. Theoretical studies are an alternative to experiments, though a reliable modeling of the electronic structures and chemical properties of plutonium-containing complexes remains a challenge for present-day quantum chemistry, as it requires treating static and dynamical correlation effects, relativistic (scalar and spin-orbit coupling) effects and eventually the influence of the species' immediate surroundings, if processes take place in solution or in the solid state.

Progresses in four-component or two-component approaches notwithstanding, a treatment of relativistic effects via one-component approaches remains computationally advantageous. [6, 7] As scalar relativistic effects are nowadays relatively straightforward to treat, and there are sufficiently accurate approaches to treat spin-orbit interactions perturbatively [8], a remaining difficulty is the large number of competing highly-correlated electronic states resulting from distributing electrons among the energetically close-lying 5f, 6d, and 7s atomic orbitals, which requires a multi-reference treatment. In addition, the so-called inner valence orbitals, 6s and 6p, are highly polarizable and yield non-negligible contribution to the electron correlation energy. [9, 10] These peculiarities in the electronic structure of actinide compounds significantly increase the computational requirements as the number of electrons that have to be considered in the correlation treatment usually exceeds the current limit of conventional multi-reference methods. [11, 12]

Several density functional theory (DFT) calculations have been performed on plutonium complexes such as oxides in the past. [9, 13–19] However, albeit DFT is in principle capable of treating open-shell molecules with multi-reference character, [20] it is known that the currently available density functional approximations often perform poorly in such cases. [12, 21] It is therefore preferable to employ from the outset multi-reference approaches such as the Complete-Active-Space Self-Consistent-Field (CASSCF) method and the Density Matrix Renormalization Group (DMRG) algorithm [22–31] in order to obtain a qualitatively correct zeroth-order wave function for these systems.

An appealing feature of the DMRG algorithm in the case of actinides and their potentially large number of quasi-degenerate states is that it allows us to include the full valence space of molecular orbitals in one single calculation without restricting the configuration space. Furthermore, when combined with concepts of quantum information theory, DMRG allows us to quantify orbital entanglement [32] and orbital-pair correlations [30, 33–39] that enable us to gain a better understanding of electron correlation effects, [36, 40, 41] elucidate chemical bonding in molecules, [37, 42–47] and detect changes in the electronic wave function. [48–50] The suitability of DMRG for helping to understand the electronic structure of actinides can be seen in a recent study of the changes in the ground-state for the CUO molecule when diluted in different noble gas matrices. [51]

The considerable body of work on actinyl species such

as PuO_2^{2+} has allowed us to be confident in our understanding of their electronic structure and the nature of the actinide–oxygen bond. [13, 17, 52–54] Using molecular orbital diagrams and accounting for point group symmetry, plutonium and oxygen can form σ and π bonds with doubly occupied orbitals up until the $3\sigma_u$ orbital. With the 5f and 6d orbitals being in the primary valence shell, actinides are able to form unique bonds and interact with other compounds in ways that no other elements are able to. [55–60] In plutonium dioxides, the 5f and 6d orbitals of the plutonium center interact with the valence orbitals on the oxygen atoms, with the exception of four pairwise degenerate nonbonding orbitals: the doubly degenerate δ_u , ϕ_u and δ_g orbitals. [55]. The bonding, antibonding, nonbonding orbitals are represented in Figure 1. This information can also be applied to neutral actinide dioxides, such as PuO_2 . [54]

However, the bonding mechanism of larger plutonium oxides and oxyhydroxides, such as PuO_3 or $\text{PuO}_2(\text{OH})_2$, is still largely unknown. For the former, its optimal geometry has been computed by Zaitsevskii *et al.* [61] using scalar relativistic DFT calculations, without mentioning the nature of the electronic ground state. In an earlier work, Gao *et al.* predicted a ${}^7\text{B}_1$ ground state, also using scalar relativistic DFT calculations, [62] but given the difficulties of DFT in treating the multi-reference character of a wave function, these findings must be cross-checked.

Our primary objective in this work is therefore to investigate in detail the electronic structure of PuO_2 , PuO_3 , and $\text{PuO}_2(\text{OH})_2$ in a scalar relativistic framework and to determine the most important valence orbitals that should be included in the active space of currently available multi-reference methods, such as CASPT2 with *a posteriori* spin-orbit coupling treatment, to ultimately compute very accurate thermodynamic properties in a forthcoming publication.

This work is organized as follows. Section II summarizes the computational details. Numerical results, including an orbital-pair correlation and entropy-based bonding analysis, are presented in section III. Finally, we conclude in section IV.

II. COMPUTATIONAL DETAILS

A. Basis set

All calculations used a relativistic effective core pseudo potential (RECP) for the plutonium center with the corresponding contracted basis set made of $(14s13p10d8f6g) \rightarrow [6s6p5d4f3g]$. [63–65] Oxygen and hydrogen atoms are described by the aug-cc-pVTZ basis sets. [66, 67] The contraction schemes are as follows: O: $(11s6p3d2f) \rightarrow [5s4p3d2f]$, H: $(6s3p2d) \rightarrow [4s3p2d]$.

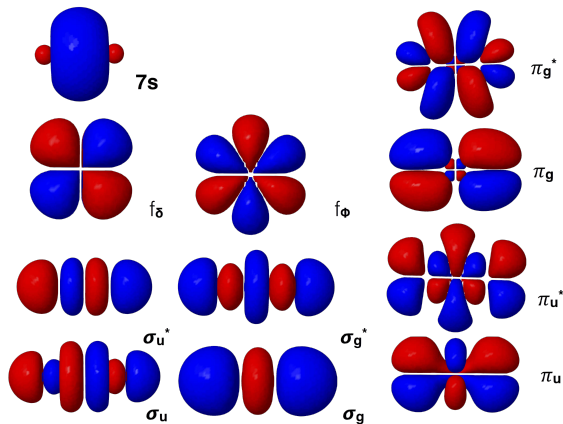


FIG. 1. Spin-free, bonding, antibonding, and nonbonding orbitals of actinyl molecule.

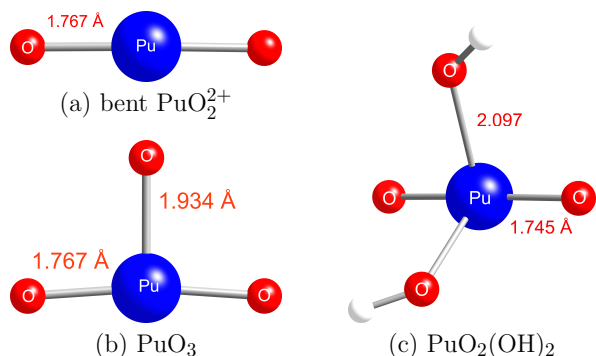


FIG. 2. Spin-free structures of all investigated plutonium oxides. The xyz coordinates of the DFT-optimized structures are summarized in the ESI.

B. Geometry Optimization

Since the exact nature of the electronic ground-states are not known for PuO_3 and $\text{PuO}_2(\text{OH})_2$, approximate structures of PuO_2 , PuO_2^{2+} , PuO_3 , and $\text{PuO}_2(\text{OH})_2$ were optimized using the GAUSSIAN09 software package to explore the properties of these oxides. [68] The B3LYP hybrid exchange-correlation functional [69] was used. The structure of the *bent* PuO_2^{2+} was obtained from the optimized PuO_3 by removing the distant oxygen. The electronic structure of PuO_2 was optimized for the quintet A_g state, while the electronic structures of all other molecules were optimized for the corresponding triplet states of B_2 and B symmetries, which were found to be most stable for the PuO_3 and $\text{PuO}_2(\text{OH})_2$ molecules, respectively. In the PuO_2^{2+} and PuO_2 molecules, the optimized bond lengths are 1.711 Å and 1.814 Å respectively. The two bond distances are different from those computed by La Macchia *et al.* due to the use of different basis sets. [54] The xyz geometries of all molecules are presented in Figure 2 and available in the ESI†.

C. CASSCF

All CASSCF [70, 71] calculations were performed using the MOLPRO2012 [72, 73] software suite. For all plutonyl molecules, *i.e.*, PuO_2^{2+} and PuO_2 , the active orbital spaces consist of δ_u , ϕ_u , and π_u^* orbitals. Specifically, for the linear and *bent* PuO_2^{2+} molecules, the active space comprises two electrons and six orbitals (CAS(2,6)SCF). The quintet ground state of the PuO_2 molecule is described by distributing four electrons in six orbitals of the active space (CAS(4,6)SCF). D_{2h} point-group symmetry was used for the linear PuO_2^{2+} and PuO_2 molecules. The energetically lowest wave-functions are the two lowest triplet states of B_{2g} and B_{3g} symmetries for PuO_2^{2+} . In the case of PuO_2 , the wave function is dominated by one single determinant ($\delta_u^{(1)}, \delta_u^{(1)}, \phi_u^{(1)}, \phi_u^{(1)}$) and of A_g symmetry with a significant configuration corresponding to the contribution of ($\phi_u^{(1)}, \phi_u^{(1)}, \pi_u^{*(1)}, \pi_u^{*(1)}$).

For both PuO_3 and $\text{PuO}_2(\text{OH})_2$, the active space contains two electrons and four orbitals (CAS(2,4)SCF). C_{2v} point-group symmetry was imposed for the *bent* PuO_2^{2+} and PuO_3 molecules, while C_2 point-group symmetry was used for $\text{PuO}_2(\text{OH})_2$. The associated triplet ground-state wave functions are of symmetry B_2 for PuO_2^{2+} and PuO_3 , and of B symmetry for $\text{PuO}_2(\text{OH})_2$, respectively. The CASSCF orbitals were visualized using the Jmol visualization software [74] and are shown in each orbital-pair correlation diagram below.

D. DMRG

The BUDAPEST DMRG [75] program was used to perform the DMRG calculations. The natural orbitals obtained from the CASSCF calculations as described in the previous subsection were used as the orbital basis.

For all DMRG calculations, the CASSCF active orbital spaces were extended by including additional occupied and virtual orbitals. For the simplest molecules, *i.e.*, PuO_2^{2+} and PuO_2 , the original CAS was extended by adding to the δ_u , ϕ_u , and π_u^* orbitals all remaining bonding and antibonding orbitals as well as the 6d $_{\delta}$ and 7s ones, resulting in a total of 25 molecular orbitals as well as 26 and 28 electrons, respectively. We will refer to these extended active spaces as the full valence CAS (FV-CAS). Furthermore, for *bent* PuO_2^{2+} , 12 occupied orbitals (5 in A_1 , 2 in B_1 , 4 in B_2 and 1 in A_2) and 8 additional virtual orbitals (3 in A_1 , 2 in B_1 , 2 in B_2 , and 1 in A_2) were added to the CASSCF active space, resulting in DMRG(26,26). For PuO_3 , we included 16 occupied orbitals (7 in A_1 , 3 in B_1 , 5 in B_2 and 1 in A_2) and 6 virtual orbitals (3 in A_1 , 2 in B_1 and 1 in B_2) with respect to CASSCF, increasing it to DMRG(34,26). The CASSCF active space of $\text{PuO}_2(\text{OH})_2$ was extended by 20 occupied orbitals (10 in A and 10 in B) and 11 virtual orbitals (6 in A and 5 in B), yielding DMRG(42,35). To facilitate our notation, all above-mentioned DMRG active spaces

will be indicated as FV-CAS.

For each molecule, we investigated a second active orbital space that was constructed by including only the strongly correlated orbitals in the DMRG active space. These strongly correlated orbitals were identified using the orbital entanglement and correlation measures obtained from DMRG calculations for the aforementioned extended full-valence active orbital spaces (orbital-pair correlation $I_{ij} > 0.01$ as a selection threshold, *vide infra*). If the size of the resulting correlation-based active space was too big or if only one orbital was close to the cut-off threshold (as in PuO_3 , bent PuO_2^{2+} , and $\text{PuO}_2(\text{OH}_2)$), we further increased our selection criterion to a value of $I_{ij} \approx 0.02$ (*vide infra*), which results in neglecting orbitals with only one major orbital-pair correlation close to the threshold of $I_{ij} \approx 0.01$. Specifically these are DMRG(14,16) for linear PuO_2^{2+} (2 in A_g , 3 in B_{3u} , 3 in B_{2u} , 3 in B_{1u} , 2 in B_{2g} , 2 in B_{3g} , and 1 in A_u), DMRG(14,15) for bent PuO_2^{2+} (4 in A_1 , 3 in B_1 , 5 in B_2 , and 3 in A_2), DMRG(18,17) for PuO_2 (1 in A_g , 4 in B_{3u} , 4 in B_{2u} , 3 in B_{1u} , 2 in B_{2g} , 2 in B_{3g} , and 1 in A_u), DMRG(14,14) for PuO_3 (4 in A_1 , 5 in B_1 , 4 in B_2 , and 1 in A_2), and finally DMRG(20,22) for $\text{PuO}_2(\text{OH})_2$ (10 in A, 12 in B). In the following, we will abbreviate those two DMRG active spaces as optCAS, indicating the optimized DMRG active space determined by means of orbital entanglement and correlation, and FV-CAS, referring to the largest DMRG active space as mentioned in the previous paragraph.

To enhance convergence, we optimized the orbital ordering. [34] The initial guess was generated using the dynamically extended-active-space procedure (DEAS). [32] For block states $m > 512$, we used the dynamic block state selection (DBSS) approach [76, 77] and set the quantum information loss $\chi = 10^{-5}$ and the minimum number of block states $m_{\min} = 512$, while the maximum number was set to $m_{\max} = \{1024, 2048\}$. All DMRG calculations are summarized in the ESI.

E. Entanglement and correlation measures

In order to select the most important active space orbitals for static/non-dynamic electron correlation, we used concepts of quantum information theory to quantify the entanglement and correlation of orbitals. Specifically, the entanglement between one orbital and all remaining orbitals is quantified by the single-orbital entropy. It can be calculated from the von Neumann entropy of the reduced density matrix of the orbital of interest, the so-called one-orbital reduced density matrix. In contrast to the N -particle reduced density matrix, which is defined for a constant number of particles, the one-orbital reduced density matrix is defined for a varying number of particles and hence its dimension is equal to the dimension of the one-orbital Fock space. In the case of spatial orbitals, we have four different one-particle states (either unoccupied, singly occupied with a spin-up or

spin-down electron, or doubly occupied orbitals) and the one-orbital reduced density matrix is a 4×4 matrix. Its elements can be calculated from the one- and two-particle reduced density matrices [39] or from generalized correlation functions. [35, 37] We refer the interested reader to refs 30, 37–39 for more details on how to calculate orbital-reduced density matrices.

The single-orbital entropy for orbital i is determined from the eigenvalues of the one-orbital reduced density matrix $\omega_{\alpha;i}$, [32]

$$s_i = - \sum_{\alpha=1}^4 \omega_{\alpha;i} \ln \omega_{\alpha;i}, \quad (1)$$

and thus represents the entanglement entropy of orbital i . Similarly, the entropy of two orbitals within the orbital bath is quantified by the two-orbital reduced density matrix as

$$s_{i,j} = - \sum_{\alpha=1}^{16} \omega_{\alpha;i,j} \ln \omega_{\alpha;i,j}, \quad (2)$$

where $\omega_{\alpha;i,j}$ are the eigenvalues of the two-orbital reduced density matrix. In contrast to the one-orbital reduced density matrix, the two-orbital reduced density matrix is defined in terms of basis states of a two-orbital Fock space, which contains 16 possible states in the case of spatial orbitals ($|--\rangle, |-\downarrow\rangle, |\downarrow-\rangle, |-\uparrow\rangle, \dots, |\uparrow\uparrow\rangle$).

Given s_i and $s_{i,j}$, we can quantify the correlation between two orbitals i and j by the orbital-pair mutual information, [32, 33, 38, 78]

$$I_{ij} = s_i + s_j - s_{i,j}, \quad (3)$$

which describes both quantum and classical correlations between two orbitals i, j . In the following, we will use diagrams to represent I_{ij} . Specifically, the strength of the orbital-pair mutual information is color-coded. Strongly correlated orbital pairs are connected by blue lines ($I_{ij} \approx 10^{-1}$), while moderately correlated orbitals are linked by red lines ($I_{ij} \approx 10^{-2}$), etc. Moreover, we will seek active orbital spaces that allow for an accurate description of static/nondynamic electron correlation effects in all investigated plutonium oxides. One possibility to define stable and reliable active spaces in correlation calculations was proposed by some of us [36, 39] and recently applied to facilitate black-box DMRG calculations. [79] In contrast to ref. 79, which uses the single-orbital entropy as exclusive selection criterion, we will exploit the orbital-pair mutual information in defining an optimal active space, primarily because I_{ij} allows us to quantify the correlation between orbital pairs and thus represents an immediate measure for electron correlation effects between orbital pairs embedded in an active space. Since we are only interested in reproducing the largest orbital-pair correlations $I_{ij} > 10^{-2}$ that are important for nondynamic/static electron correlation, the orbital-pair correlation-based active space will be constructed by excluding all orbitals for which all values

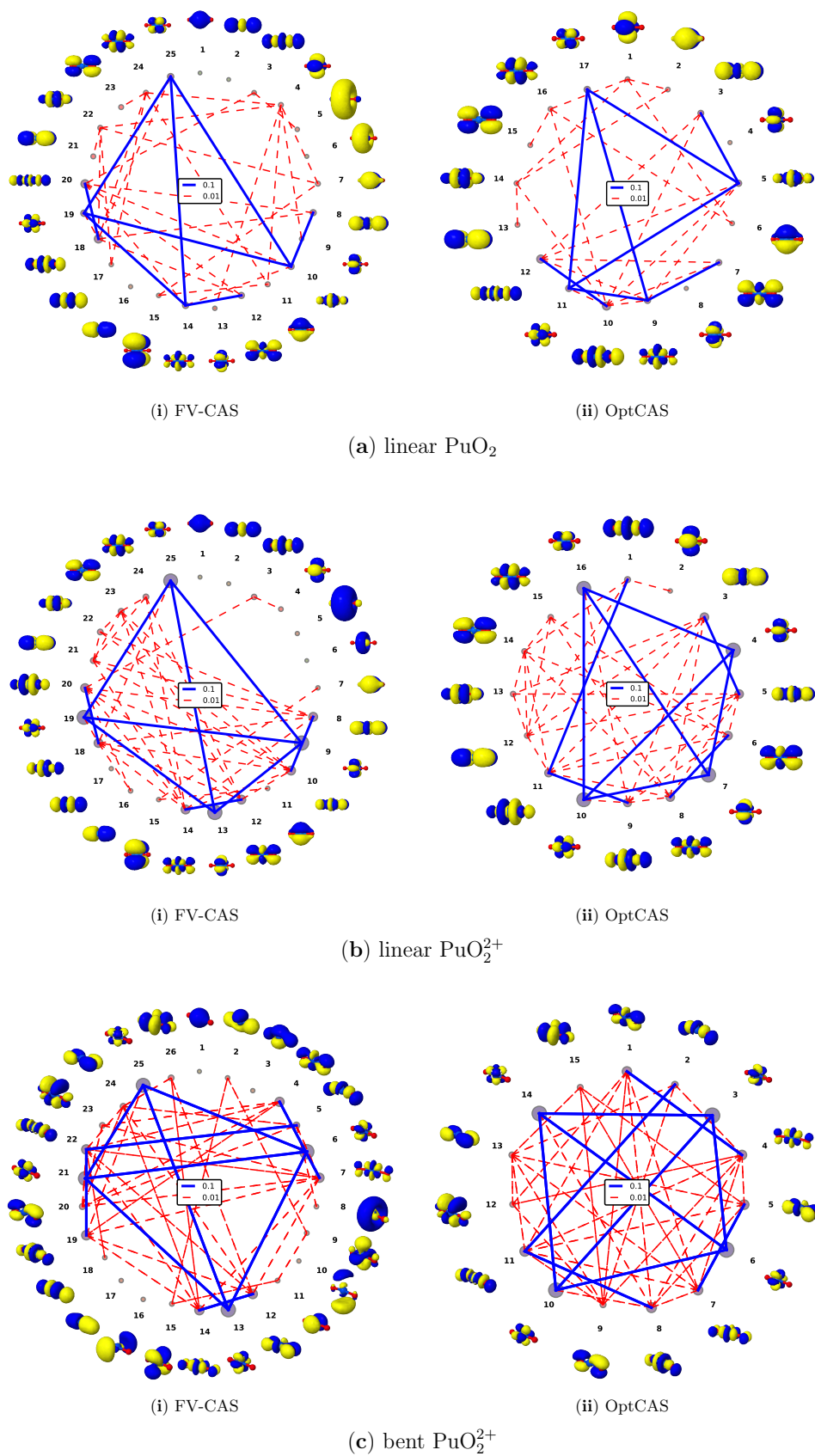


FIG. 3. Orbital correlations for the PuO_2 molecule and linear and *bent* PuO_2^{2+} ions and two different active spaces. The strength of the orbital-pair correlations is color-coded: the strongest orbital-pair correlations are marked by blue lines (10^{-1}), followed by orbital-pair correlations linked by red lines (10^{-2}).

of the orbital-pair mutual information are smaller than 10^{-2} . If the resulting active orbital spaces are stable, we should recover the largest orbital-pair correlations with respect to the reference calculations. Otherwise, the acceptance threshold for $I_{i|j}$ has to be further reduced (for instance, to 10^{-3}). In this work, a cutoff threshold for $I_{i|j}$ of 0.01 was, however, sufficient in reproducing the dominant orbital-pair correlations and we did not perform additional calculations with smaller thresholds for $I_{i|j}$. The error introduced by decreasing the size of the active space can be quantified by determining, for instance, the squared deviation of orbital-pair correlations for the optimized active orbital space, here optCAS, with respect to the reference active space, here FV-CAS,

$$\varepsilon_{\text{optCAS}} = \sum_{i,j \in \text{optCAS}} \left(I_{i|j}^{\text{FV-CAS}} - I_{i|j}^{\text{optCAS}} \right)^2. \quad (4)$$

In this work however, we focus only on the distribution of $I_{i|j}$ determined for different CASs to assess the reliability of the reduced active orbital spaces. Finally, we should emphasize that we use two-orbital correlation measures to study the electronic structures and bonding patterns in plutonium oxides. An extension to multi-orbital correlations has been presented recently in Ref. 80.

III. RESULTS AND DISCUSSION

Since the detailed bonding mechanisms of the larger plutonium oxides PuO_3 and $\text{PuO}_2(\text{OH})_2$ are unknown, we will compare the properties on the *bent* PuO_2^{2+} molecule as a possible subunit of the PuO_3 and $\text{PuO}_2(\text{OH})_2$ complexes. As a preliminary step, we will focus on the linear PuO_2 and PuO_2^{2+} species. Specifically, we will scrutinize how the addition of the distant oxygen atom to the PuO_2^{2+} moiety influences orbital correlations and bonding patterns when going from PuO_2^{2+} to PuO_3 . Then, we will discuss how the electronic structure changes when two hydroxy groups are added to the PuO_2^{2+} subunit forming the $\text{PuO}_2(\text{OH})_2$ molecule.

A. The PuO_2 molecule

According to La Macchia *et al.*, spin-orbit coupling induces a change in the principle electronic configuration; at the spin-orbit level, it is 96 % dominated by a $^5\phi_u$ spin-free state, *i.e.*, the dominant configuration is $7s^{(1)}\delta_u^{(2)}\phi_u^{(2)}$. [54] However at the spin-free level, the ground state is a $^5\Sigma_g^+$ that lies 1800 cm^{-1} below the $^5\phi_u$ state, and corresponds to the single occupation of the δ_u and ϕ_u molecular orbital pairs. Thus, in this study we will consider only the spin-free $^5\Sigma_g^+$ state and analyse its DMRG matrix product state wave function. The latter is described by a single determinant as shown by the wavefunction analysis at the CASSCF level, that could be decomposed into two major determinants, $|\delta_u^{(1)}\delta_u^{(1)}\phi_u^{(1)}\phi_u^{(1)}\rangle$

and $|\phi_u^{(1)}\phi_u^{(1)}\pi_u^{(1)}\pi_u^{(1)}\rangle$, with a weight of 90 % and 8 %, respectively.

The most important orbital-pair correlations for the linear PuO_2 molecule and all investigated orbital spaces are shown in Fig. 3(a). The dominant orbital correlations as obtained from the optCAS calculation are in good agreement with the correlation diagram of the FV-CAS reference, indicating that static/nondynamic electron correlation effects are accurately captured in the optCAS active space.

To highlight the good agreement in orbital correlations between FV-CAS and optCAS, Fig. 4 shows the sorted, decaying values of the orbital-pair mutual information for the first 50 strongly correlated orbital pairs. For better comparison, we use the same color-coding scheme for the strength of the orbital-pair mutual information as displayed in Fig. 3. Each $I_{i|j}$ in Fig. 4 is shown for the same orbital pair i, j and sorted with respect to the FV-CAS reference values. As shown in Fig. 4(a), optCAS results in a distribution of orbital correlations that is similar to the FV-CAS reference distribution, with 8 dominant distributions over 10^{-1} , and one at the limit with a squared deviation of $\varepsilon_{\text{optCAS}} = 0.00128$.

For both optCAS and FV-CAS, the seven of the eight distributions correspond to strong pair-correlation between the bonding and antibonding π_u/π_u^* orbitals (nos. 3, 5, 7 and 9 in Fig. 3(a-ii)) (2 blue lines) as well as the antibonding π_u/π_u^* orbitals and the two nonbonding δ_u orbitals (nos. 11 and 17 in Fig. 3(a-ii); 4 blue lines) and the two nonbonding δ_u (1 blue line). Specifically, the bonding and antibonding combination of both oxygen p_z orbitals and the plutonium f_{z^3} orbital lead to the formation of a σ_u bond between the plutonium center and the oxygen atoms, which results in one strongly correlated $\sigma_u-\sigma_u^*$ orbital pair (nos. 10 and 12 in Fig. 3(a-ii)). Note that the doubly degenerate ϕ_u orbitals have $I_{i|j}$ values much smaller than 10^{-3} . Even so, the entanglement with other antibonding orbitals remains weak, the population analysis (cf Table S2 in the ESI) exhibits a single occupation of the ϕ_u orbitals, making them obviously important in the description of the ground-state. Thus one can conclude that the remaining σ_u/σ_u^* , π_u/π_u^* , and δ_u as well as ϕ_u orbitals are important to describe nondynamic/static electron correlation appropriately. The last statement conforms to the choice of La Macchia *et al.* not to consider the π_g and σ_g^* molecular orbitals in their active space. [54]

B. The plutonyl PuO_2^{2+} ion

1. The linear structure

The electronic structure of the linear PuO_2^{2+} complex was optimized in its triplet ground state that consists of a linear combination of two determinants with equal weights, $|\phi_u^{(1)}(\text{B}_{3u})\delta_u^{(1)}(\text{B}_{1u})\rangle$ and $|\phi_u^{(1)}(\text{B}_{2u})\delta_u^{(1)}(\text{A}_u)\rangle$.

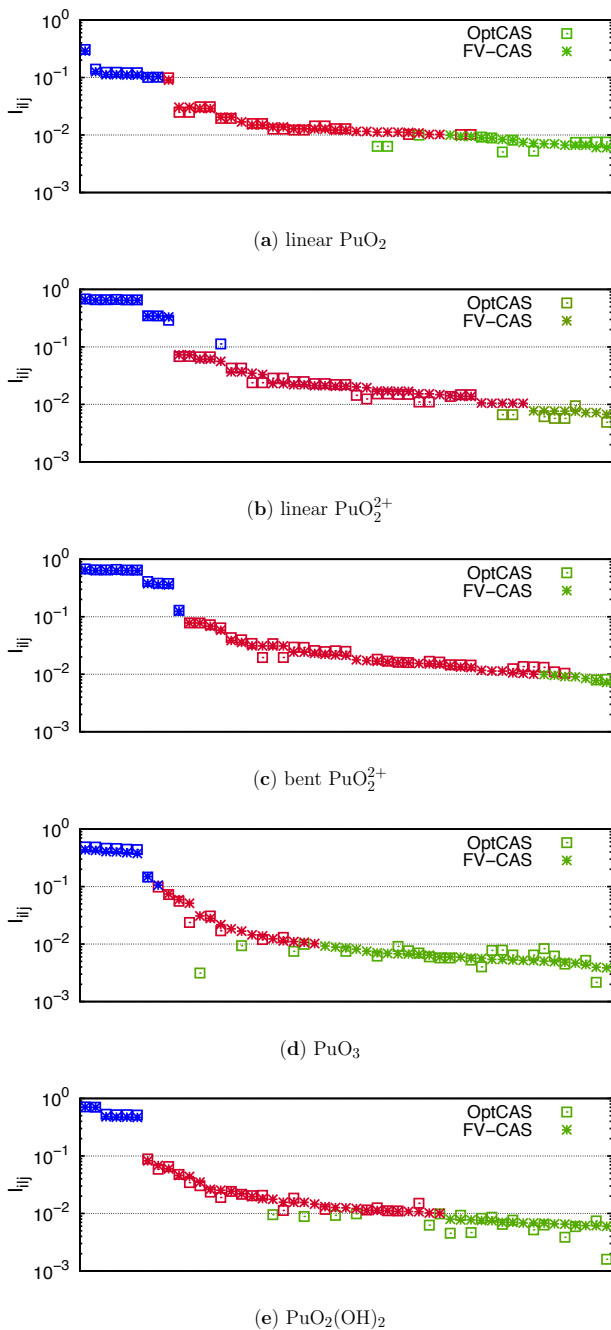


FIG. 4. Decaying values for the orbital-pair mutual information for all investigated plutonium oxide complexes and different active spaces. The values of the mutual information are ordered with respect to the FV-CAS reference calculation, *that is*, each I_{ij} is plotted for the same indices i and j of FV-CAS and optCAS.

The orbital-pair correlations are displayed in Fig. 3(b) for both active spaces studied. In the optCAS calculation, the orbital-pair correlations are identical to that of the large FV-CAS reference calculation (compare Figs. 3(b-i) and (b-ii)). The good agreement of optCAS and FV-CAS in describing static/nondynamic

electron correlation is also evident in the decay of the orbital-pair mutual information shown in Fig. 4(b). In general, differences in orbital-pair correlations between optCAS and FV-CAS are negligible. The largest differences are found for weakly correlated orbital-pairs, which can be attributed to dynamic electron correlation effects beyond the optCAS orbitals, and between the σ_g and σ_g^* orbitals (nos. 1 and 11 in Fig. 3(b-ii)), which are slightly over-correlated in the optCAS calculation as compared to the FV-CAS and lead to a larger squared deviation of $\varepsilon_{\text{optCAS}} = 0.00800$ compared to PuO_2 . Nonetheless, similar I_{ij} profiles for optCAS and FV-CAS suggest the proper choice of the optCAS active space.

Similarly to the linear PuO_2 molecule, the strongly-correlated orbital pairs are the singly-occupied δ_u (nos. 10 and 16 in Fig. 3(b-ii)) orbitals as well as the bonding and antibonding combination of the π_u orbitals (nos. 3 and 5 as well as 6 and 8 in Fig. 3(b-ii)) and the σ_u orbitals (nos. 9 and 11 in Fig. 3(b-ii)). However, in contrast to PuO_2 , the doubly-degenerate (and nonbonding) ϕ_u orbitals (nos. 4 and 7 in Fig. 3(b-ii)) become strongly correlated with the δ_u orbitals, while the pair-correlation between the π_u and δ_u decreases with I_{ij} values below 10^{-2} . Furthermore, like in linear PuO_2 , the π_u and π_u^* orbitals (nos. 3 and 5 as well as 6 and 8 in Fig. 3(b-ii)) are more strongly correlated than the π_g - π_g^* orbital pair (nos. 12 and 13 as well as 14 and 15 in Fig. 3(b-ii)). The different strength of correlation between the π_u/π_u^* and π_g/π_g^* orbitals is also observable in the abrupt decrease in orbital-pair mutual information around 10^{-1} (see Fig. 4(b)). Finally, to account properly for static/nondynamic electron correlation, a CASSCF calculation should include, as for the PuO_2 molecule, the σ_u/σ_u^* , π_u/π_u^* , and δ_u as well as ϕ_u orbitals.

2. The bent structure

For simplicity and in the following sections, the orbital labels were kept identical to those referring to D_{2h} symmetry. Distorting the structure of the linear PuO_2^{2+} molecule into the *bent* PuO_2^{2+} subunit present in PuO_3 and $\text{PuO}_2(\text{OH})_2$ changes the orbital-pair correlation picture marginally. As observed for the linear $\text{PuO}_2/\text{PuO}_2^{2+}$, the strongly correlated orbital pairs are the singly-occupied δ_u and ϕ_u (nos. 3, 6, 10, and 14 in Fig. 3(c-ii)) orbitals as well as both π_u/π_u^* orbitals (nos. 1 and 4 as well as 5 and 7 in Fig. 3(c-ii)) and the σ_u/σ_u^* orbitals (nos. 8 and 11 in Fig. 3(c-ii)). Furthermore, the π_g - π_g^* orbital pairs (nos. 9 and 12 as well as 13 and 15 in Fig. 3(c-ii)) remain moderately correlated as in the linear PuO_2^{2+} counterpart. Bending the $\text{Pu}\equiv\text{O}$ bond increases, however, the orbital-pair correlation between the σ_g and σ_u orbitals (nos. 2 and 11 in Fig. 3(c-ii)) by approximately one order of magnitude. Thus, in order to describe the strongest orbital-pair correlations for *bent* PuO_2^{2+} , the σ_g orbital has to be included in the active space. As observed above, the differences in orbital-pair

correlations between optCAS and FV-CAS are negligible with $\varepsilon_{\text{optCAS}} = 0.00523$.

The most pronounced differences in orbital-pair correlations can be found for σ -type orbitals. Since, however, only one orbital-pair correlation is affected (cf., Figs. 5(b) and (c)), the structural distortion can be considered too small to have a significant impact on the σ - and π -bonding mechanisms in PuO_2^{2+} .

C. The PuO_3 molecule

In contrast to structural distortions, addition of the distant O^{2-} group to the *bent* PuO_2^{2+} subunit changes the orbital-pair correlations. Similar to the *bent* PuO_2^{2+} subunit, the plutonium δ_u and ϕ_u orbitals of PuO_3 are highly correlated with each other, while the remaining active space orbitals are moderately to weakly correlated (see Fig. 5(a)), especially the σ_u - σ_u^* and π_u - π_u^* orbital pairs that decrease below the threshold of 10^{-1} in the optCAS. Although weak correlations ($I_{ij} \leq 10^{-2}$) are underestimated in our optCAS calculations compared to the FV-CAS reference (see Fig. 4(c)), optCAS still represents the smallest active space that contains all important orbitals to reliably describe nondynamic/static electron correlation. We should note, however, that the squared deviation increases to $\varepsilon_{\text{optCAS}} = 0.02389$ because we have increased the cutoff threshold for the orbital-pair mutual information to $I_{ij} \approx 0.02$, excluding orbital no. 5 in Fig. 5(a-ii).

The orbital-pair correlation diagrams can be further used to elucidate how the bonding mechanism in PuO_3 changes compared to the PuO_2^{2+} subunit. In the PuO_3 molecule, the singly occupied plutonium δ_u and ϕ_u orbitals are strongly correlated (nos. 3, 7, 12, and 14 in Fig. 5(a-ii)), with orbital-pair mutual information similar in magnitude to the δ_u/ϕ_u correlations in PuO_2^{2+} . Furthermore, in contrast to the strongly correlated $\sigma_u - \sigma_u^*$ orbital pair in the $\text{PuO}_2/\text{PuO}_2^{2+}$ molecules, the $\sigma_u - \sigma_u^*$ orbitals are only moderately correlated (nos. 10 and 13 in Fig. 5(a-ii)) in PuO_3 .

We observe that only the π_u and π_u^* orbitals out of the plane defined by the molecule are still strongly correlated (nos. 13 and 17 in Fig. 5(a-i) with 1 blue line and nos. 5 and 9 in Fig. 5(a-ii) with 1 red line), while the π_u and π_u^* orbitals located in the plane are only weakly correlated (nos. 5 and 20 in Fig. 5(a-i), not shown in the Figure). More striking is the important orbital-pair correlation between the p_z orbital of the distant oxygen with the δ_u orbital (nos. 22 and 23 in Fig. 5(a-i)), and the weaker ones with the planar bonding π_u orbital (no. 20 in Fig. 5(a-i)) and the hybrid antibonding orbital constructed as a combination of the planar π_u^* MO and the distant-oxygen p_x orbital (no. 2 in Fig. 5(a-ii)); the later being coupled with the ϕ_u orbital (no. 3 in Fig. 5(a-i))

An interesting feature concerns the orbitals that describe the bonding between the distorted plutonyl subunits and the distant oxygen. The bonding and anti-

bonding orbitals forming σ -type orbitals (nos. 2 and 4 in Fig. 5(a-i)) do not contribute at all in the description of the ground-state wave-function. Hence, we can assume that the axial π bond is not formed by the plutonium π_u and oxygen p_z orbitals. Instead, the axial and equatorial oxygen p_z orbitals interact with the plutonium $6d_\sigma$ orbital (no. 2 in Fig. 5(a-ii)) and the corresponding molecular orbital can be considered as a hybrid of an axial plutonium–oxygen σ bond and δ_u -type bonding between the three oxygen atoms. This σ/δ_u -type molecular orbital is moderately correlated with the singly occupied plutonium ϕ_u orbital. The remaining p orbitals of the axial oxygen atom slightly mix with plutonium $6d$ orbitals (nos. 6 and 11 in Fig. 5(a-ii)) and become moderately correlated with the plutonium ϕ_u and δ_u orbitals.

The strong discrepancies in I_{ij} between optCAS and FV-CAS can be explained by investigating the electronic structure of PuO_3 . In contrast to the PuO_2^{2+} subunit, the electronic structure of PuO_3 is dominated by dynamic electron correlation effects beyond the optCAS orbitals, which results in I_{ij} being underestimated in comparison to the FV-CAS reference distribution (see Fig. 4(c)). However, the missing dynamic electron correlation effects do not considerably affect the nondynamic/static correlation in the (optCAS) active space and can be included *a posteriori* using, for instance, perturbation theory.

Note that nondynamic/static electron correlation effects can be accurately described within the optCAS, which contains the distant-oxygen p orbitals and the other orbitals of the distorted plutonyl subunit. Hence, a minimal active space containing the σ_u/σ_u^* , π_u/π_u^* , and δ_u as well as ϕ_u orbitals and the p -shell of the oxygen would suffice to accurately model the ground-state wave function in PuO_3 .

D. The $\text{PuO}_2(\text{OH})_2$ complex

As observed for the PuO_3 complex, extending the ligand sphere of PuO_2^{2+} with two hydroxy groups changes the orbital-pair correlations compared to the triatomic subunit. In the $\text{PuO}_2(\text{OH})_2$ molecule, the singly-occupied δ_u and ϕ_u orbitals (nos. 5, 6, 16, and 17 in Fig. 5(b-ii)) are strongly correlated, while the plutonium π_g and π_u orbitals are moderately correlated. To describe nondynamic/static electron correlation appropriately, the active space can be reduced from 35 (FV-CAS) to 22 (OptCAS) orbitals without changing orbital-pair correlations (see also Fig. 4(d)). Although some orbital-pair correlations with $I_{ij} \approx 10^{-2}$ are underestimated, the orbital-pair mutual information for $I_{ij} > 10^{-2}$ determined from optCAS agrees well with the FV-CAS reference distribution (see Fig. 4(d)) with a squared deviation of $\varepsilon_{\text{optCAS}} = 0.01030$. The discrepancies in I_{ij} between optCAS and FV-CAS can be attributed to dynamic correlations effects outside the optCAS active space. However, they do not influence the orbital-pair correlations where $I_{ij} \gg 10^{-2}$. Thus, optCAS with 20 electrons

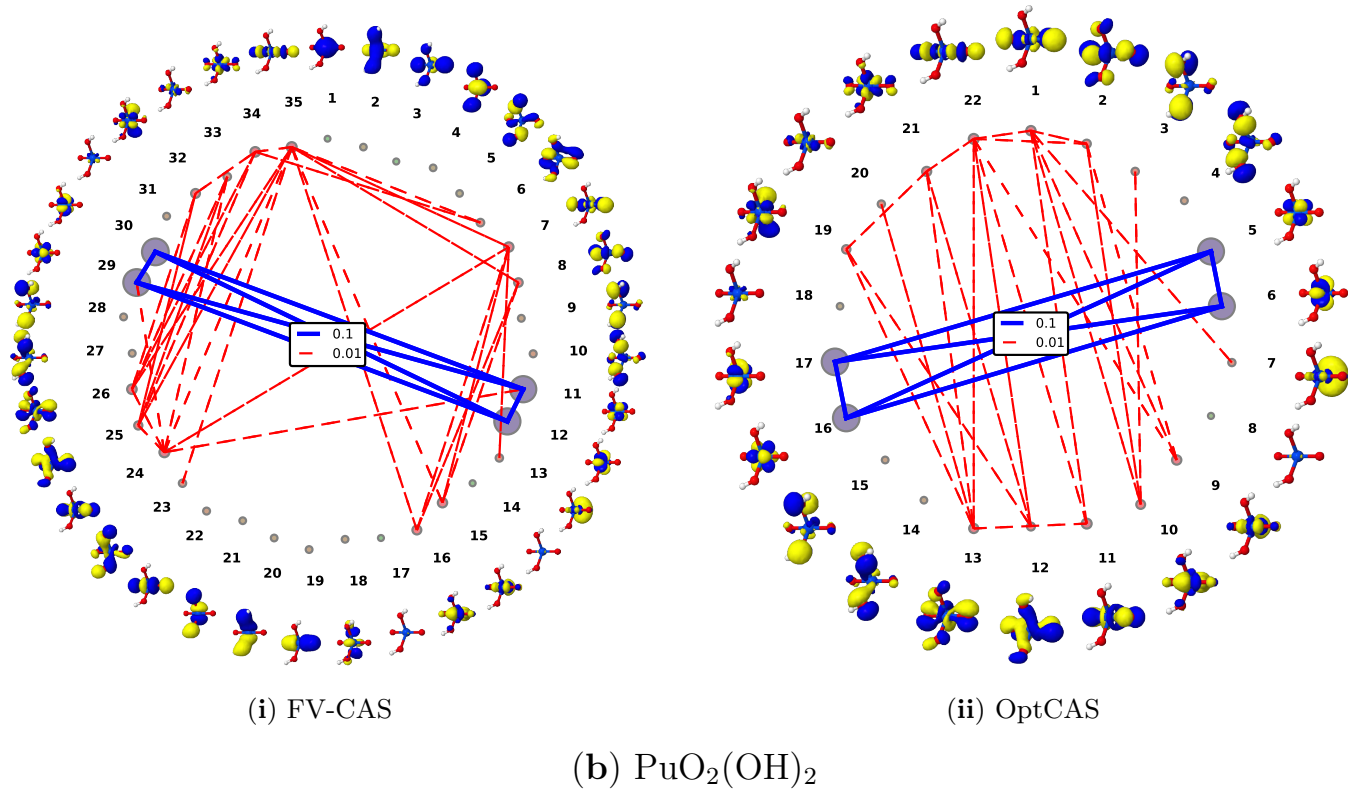
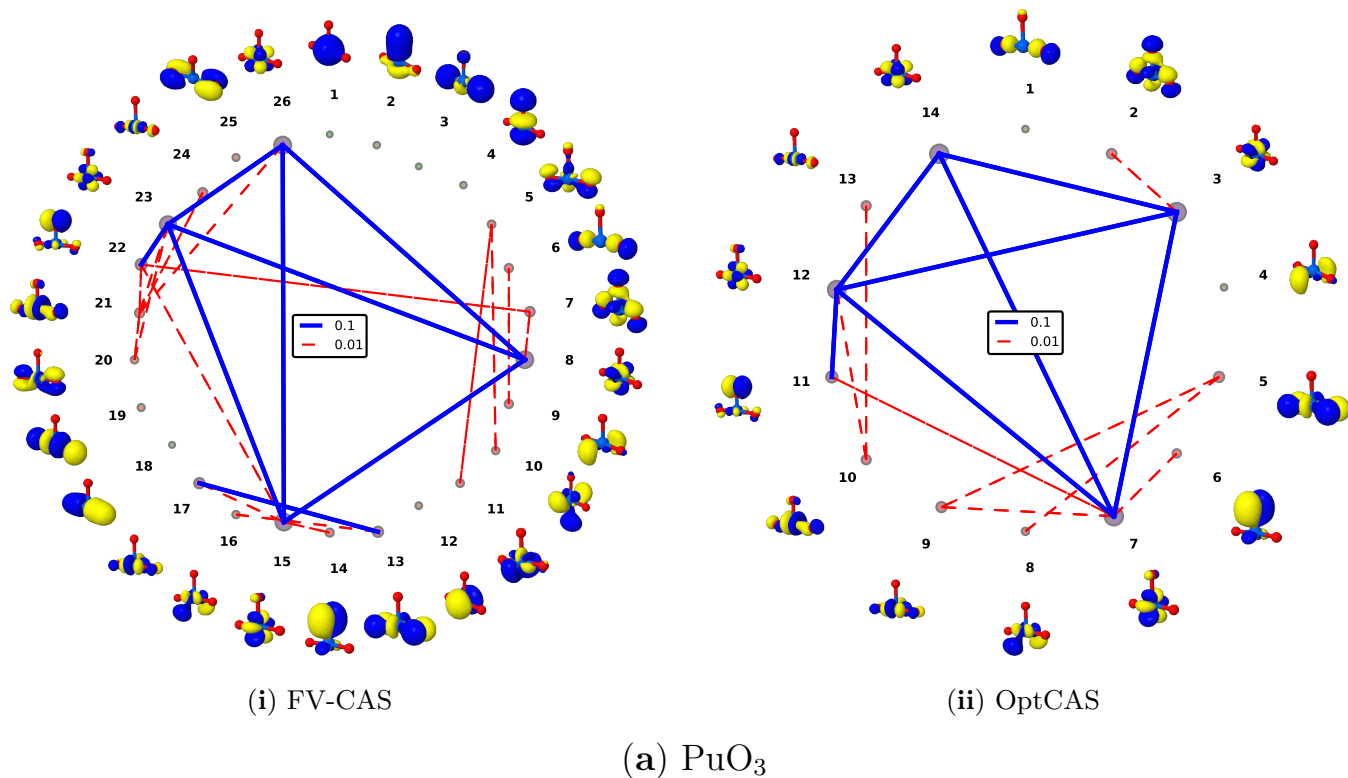


FIG. 5. Orbital correlations for the PuO_3 and $\text{PuO}_2(\text{OH})_2$ molecules and two different active spaces. The strength of the orbital-pair correlations is color-coded: the strongest orbital-pair correlations are marked by blue lines (10^{-1}), followed by orbital-pair correlations linked by red lines (10^{-2}).

correlated in 22 orbitals represents a good choice to describe the most important correlation effects present in the $\text{PuO}_2(\text{OH})_2$ molecule. Note that optCAS could be further reduced by excluding 5 molecular orbitals (nos. 4, 8, 14, 15, and 18 in Fig. 5(b-ii)) as those orbitals are not important for static/nondynamic electron correlation. Since, however, those orbitals lie energetically between the other active space orbitals, we have kept them in our optCAS calculations. If we neglect changes in orbital-pair correlations due to minor structural differences in the PuO_2^{2+} subunit, we can conclude that the addition of two hydroxy ligands decreases nondynamic/static electron correlation effects in the $\text{PuO}_2(\text{OH})_2$ complex compared to the bare PuO_2^{2+} model compound (compare Figs. 4(b) and (d)). Furthermore, we observe the most profound jump in the mutual information around $I_{i|j} \approx 10^{-2}$ in the $\text{PuO}_2(\text{OH})_2$ molecule which stresses how additional ligands influence orbital-pair correlations in the PuO_2^{2+} unit.

In contrast to the PuO_2 and PuO_2^{2+} units, the plutonium 5f and 6d orbitals hybridize considerably with each other as well as with all oxygen p orbitals. Specifically, the plutonium 5f/6d orbitals mix with the oxo p orbitals to form moderately correlated f/d_π and f/d_{π^*} -type orbitals (nos. 9, 13, 21, and 22 in Fig. 5(b-ii)), while the hydroxy p orbitals mix with the oxo p orbitals and the plutonium 5f/6d orbitals to form molecular orbitals (nos. 2 and 12 in Fig. 5(b-ii)) that are moderately correlated with the f/d_π and f/d_{π^*} -type orbitals. This reduces the $\pi_u-\pi_u^*$ orbital-pair correlations as observed in the PuO_2^{2+} unit. Furthermore, the orbital-pair correlation of the $\sigma-\sigma^*$ orbital pair (nos. 1 and 11 in Fig. 5(b-ii)) weakens when going from the bare PuO_2^{2+} molecule to $\text{PuO}_2(\text{OH})_2$. Finally, the hydroxy lone-pairs (nos. 3, 4, 14, and 15 in Fig. 5(b-ii)) are only weakly correlated ($I_{i|j} < 10^{-2}$) with molecular orbitals centered on the PuO_2^{2+} subunit, which are thus not shown in the Figure.

Therefore, we can conclude that the π bonding mechanism changes most significantly when two hydroxy groups are added to the bare PuO_2^{2+} complex. A similar observation was already made for the PuO_3 compound discussed above. Specifically, the plutonium 5f and 6d orbitals mix considerably and form bonding and antibonding f/d_π orbitals with the oxo p orbitals. These hybrid f/d_π orbitals contribute to the π bonding in the PuO_2^{2+} subunit of the $\text{PuO}_2(\text{OH})_2$ molecule. Furthermore, the orbital-pair correlation diagrams suggest that the hydroxy ligands mainly interact with the PuO_2^{2+} subunit through hydroxo p and plutonium f/d mixing which alters the π_g bonding interaction of the bare PuO_2^{2+} molecule and reduces the $\pi_g-\pi_g^*$ orbital-pair correlation in the hydroxyligated PuO_2^{2+} complex. Thus, the bonding mechanisms in the $\text{PuO}_2(\text{OH})_2$ compound are a complex interplay of plutonium 5f and 6d orbitals, the oxo $2p$ orbitals, and the oxygen $2p$ orbitals of the hydroxo ligands.

IV. CONCLUSIONS

Actinide-containing compounds are remarkably challenging for present-day quantum chemistry, primarily because of the large number of the energetically close 5f, 6d, and 7s orbitals that have to be included in active space calculations as well as the need to account for relativistic effects in the quantum-chemical model. In this work, we have investigated the electronic structure and bonding mechanisms of different plutonium oxides using the DMRG algorithm and concepts of quantum information theory.

For each plutonium compound, we studied two different active orbital spaces: a large (full-valence) active space (FV-CAS) and an active space that reproduces the most important nondynamic/static orbital-pair correlations of this FV-CAS reference calculation, but simultaneously, allows us to reduce the number of active space orbitals as much as possible (here, called optCAS). The orbital-pair mutual information, used to select the most important active space orbitals from a large active space reference calculation, allows us to dissect electron correlation effects and easily identify those orbitals that are important for nondynamic/static and weak correlation, respectively. [36]

Thus, an optimal active space can be defined by only selecting the strongly correlated orbitals, from a large active space calculation that reproduces the orbital-pair correlation diagram of the reference calculation, resulting in DMRG(14,16) for linear PuO_2^{2+} , DMRG(14,15) for *bent* PuO_2^{2+} , DMRG(18,17) for linear PuO_2 , DMRG(14,14) for PuO_3 , and finally DMRG(20,22) for $\text{PuO}_2(\text{OH})_2$. Most importantly, the discrepancies in $I_{i|j}$ between optCAS and FV-CAS are minor and are caused by dynamic electron correlation effects beyond the optCAS active space orbitals. Thus, optCAS should result in reliable zeroth-order wave function for an *a posteriori* treatment of dynamic electron correlation effects.

Our results also serve to underscore the differences in the bonding picture for PuO_3 and $\text{PuO}_2(\text{OH})_2$ with respect to the bare plutonyl species. For both molecules, the π -bonding mechanism changes significantly when oxo or hydroxo ligands are added to the triatomic plutonyl unit. Specifically for $\text{PuO}_2(\text{OH})_2$, we observe considerable changes with respect to plutonyl, with substantial mixing of the plutonium 5f and 6d orbitals that results in two bonding and anti bonding hybrid f/d_π orbitals, with the orbital-pair correlation analysis indicating that the hydroxo and plutonyl subunits interact through mixing of plutonium f/d and hydroxo p orbitals, which reduces the $\pi_g-\pi_g^*$ correlation found in PuO_2^{2+} . Thus, concepts of quantum information theory represent a rich and useful tool to perform electronic structure calculations, to interpret electronic wave functions, and to gain chemical insights into the structure of molecules that are difficult to understand using standard approaches like molecular orbital diagrams. Most importantly, our approach can be reliably applied whenever the electronic wave func-

tion can be accurately optimized, even in cases when the simple picture of interacting orbitals completely fails.

V. ACKNOWLEDGEMENT

We gratefully acknowledge financial support from the France-Canada Research Fund, Natural Sciences and Engineering Research Council of Canada (NSERC), and the Hungarian Research Fund (OTKA K100908 and NN110360). The members of the PhLAM laboratory acknowledge support from the CaPPA project (Chemical and Physical Properties of the Atmosphere) that is funded by the French National Research Agency (ANR) through the PIA (Programme d'Investissement d'Avenir) under contract "ANR-11-LABX-0005-01" and by the Regional Council "Hauts de France" and

the "European Funds for Regional Economic Development (FEDER) C.D. acknowledges financial support from the NSERC Undergraduate Student Research Award fellowship. K.B. acknowledges financial support from a SONATA BIS grant of the National Science Centre, Poland (no. 2015/18/E/ST4/00584) and a Marie-Sklodowska-Curie Individual Fellowship project no. 702635-PCCDX. P.T. thanks the National Science Center Grant No. DEC-2013/11/B/ST4/00771 and No. DEC-2012/07/B/ST4/01347.

The authors acknowledge support for computational resources from SHARCNET, a partner consortium in the Compute Canada national HPC platform. Calculations have been carried out using resources provided by Wroclaw Centre for Networking and Supercomputing (<http://wcss.pl>), grant No. 10105802.

-
- [1] J. Hartmann, *Nat. Chem.*, 2012, **4**, 1052.
- [2] R. G. Haire and J. M. Haschke, *MRS Bull.*, 2001, **26**, 689–696.
- [3] K. L. Nash, *Solvent Extr. Ion Exch.*, 1993, **11**, 729–768.
- [4] K. L. Nash, R. E. Barrans, R. Chiarizia, M. L. Dietz, M. Jensen, P. Rickert, B. A. Moyer, P. V. Bonnesen, J. C. Bryan and R. A. Sachleben, *Solvent Extr. Ion Exch.*, 2000, **18**, 605–631.
- [5] C. Ronchi, F. Capone, J. Y. Colle and J. P. Hiernaut, *J. Nucl. Mat.*, 2000, **280**, 111–115.
- [6] M. Reiher and A. Wolf, *Relativistic Quantum Chemistry. The Fundamental Theory of Molecular Science*, Wiley, Dordrecht, 2009.
- [7] P. Tecmer, K. Boguslawski and D. Kędziera, in *Handbook of Computational Chemistry*, ed. J. Leszczyński, Springer Netherlands, Dordrecht, 2016, pp. 1–43.
- [8] V. Vallet, L. Maron, C. Teichteil and J.-P. Flament, *J. Chem. Phys.*, 2000, **113**, 1391–1402.
- [9] G. Schreckenbach and G. A. Shamov, *Acc. Chem. Res.*, 2010, **43**, 19–29.
- [10] A. S. P. Gomes, F. Réal, B. Schimmelpfennig, U. Wahlgren and V. Vallet, in *Applied Computational Actinide Chemistry*, ed. M. Dolg, John Wiley & Sons Ltd, Chichester, 2015, ch. 11, pp. 269–298.
- [11] L. Maron, T. Leininger, B. Schimmelpfennig, V. Vallet, J.-L. Heully, C. Teichteil, O. Gropen and U. Wahlgren, *Chem. Phys.*, 1999, **244**, 195–201.
- [12] C. Clavaguéra-Sarrio, V. Vallet, D. Maynau and C. J. Marsden, *J. Chem. Phys.*, 2004, **121**, 5312–5321.
- [13] N. Ismail, J.-L. Heully, T. Saue, J.-P. Daudey and C. J. Marsden, *Chem. Phys. Lett.*, 1999, **300**, 296.
- [14] P. J. Hay, R. L. Martin and G. Schreckenbach, *J. Phys. Chem. A*, 2000, **104**, 6259–6270.
- [15] S. O. Odoh and G. Schreckenbach, *J. Phys. Chem. A*, 2010, **114**, 1957.
- [16] A. Kovács and R. J. M. Konings, *J. Phys. Chem. A*, 2011, **115**, 6646–6656.
- [17] A. Kovács, P. Pogány and R. J. M. Konings, *Inorg. Chem.*, 2012, **51**, 4841–4849.
- [18] W. Huang, W.-H. Xu, J. Su, W. H. E. Schwarz and J. Li, *Inorg. Chem.*, 2013, **52**, 14237–14245.
- [19] A. Kovács, R. J. M. Konings, J. K. Gibson, I. Infante and L. Gagliardi, *Chem. Rev.*, 2015, **115**, 1725–1759.
- [20] D. Cremer, M. Filatov, V. Polo, E. Kraka and S. Shaik, *Int. J. Mol. Sci.*, 2002, **3**, 604–638.
- [21] A. S. P. Gomes, F. Réal, N. Galland, C. Angeli, R. Cimiraglia and V. Vallet, *Phys. Chem. Chem. Phys.*, 2014, **16**, 9238–9248.
- [22] S. R. White, *Phys. Rev. Lett.*, 1992, **69**, 2863–2866.
- [23] S. R. White, *Phys. Rev. B*, 1993, **48**, 10345–10356.
- [24] S. R. White and R. L. Martin, *J. Chem. Phys.*, 1999, **110**, 4127–4130.
- [25] U. Schollwöck, *Rev. Mod. Phys.*, 2005, **77**, 259–315.
- [26] Ö. Legeza, R. Noack, J. Sólyom and L. Tincani, in *Computational Many-Particle Physics*, ed. H. Fehske, R. Schneider and A. Weiße, Springer, Berlin/Heidelberg, 2008, vol. 739, pp. 653–664.
- [27] K. H. Marti and M. Reiher, *Z. Phys. Chem.*, 2010, **224**, 583–599.
- [28] G. K.-L. Chan and S. Sharma, *Annu. Rev. Phys. Chem.*, 2011, **62**, 465–481.
- [29] S. Wouters and D. Van Neck, *Eur. Phys. J. D*, 2014, **68**, 272.
- [30] S. Szalay, M. Pfeiffer, V. Murg, G. Barcza, F. Verstraete, R. Schneider and Ö. Legeza, *Int. J. Quantum Chem.*, 2015, **115**, 1342–1391.
- [31] T. Yanai, Y. Kurashige, W. Mizukami, J. Chalupsky, T. N. Lan and M. Saitow, *Int. J. Quantum Chem.*, 2015, **115**, 283–299.
- [32] Ö. Legeza and J. Sólyom, *Phys. Rev. B*, 2003, **68**, 195116.
- [33] J. Rissler, R. M. Noack and S. R. White, *Chem. Phys.*, 2006, **323**, 519–531.
- [34] G. Barcza, Ö. Legeza, K. H. Marti and M. Reiher, *Phys. Rev. A*, 2011, **83**, 012508.
- [35] Ö. Legeza, G. Barcza, R. M. Noack and J. Sólyom, Entanglement topology of strongly correlated systems, Korrlationstage MPIPKS, Dresden, 2013.
- [36] K. Boguslawski, P. Tecmer, Ö. Legeza and M. Reiher, *J. Phys. Chem. Lett.*, 2012, **3**, 3129–3135.
- [37] K. Boguslawski, P. Tecmer, G. Barcza, Ö. Legeza and M. Reiher, *J. Chem. Theory Comput.*, 2013, **9**, 2959–2973.

- [38] G. Barcza, R. Noack, J. Sólyom and Ö. Legeza, *Phys. Rev. B*, 2014, **92**, 125140.
- [39] K. Boguslawski and P. Tecmer, *Int. J. Quantum Chem.*, 2015, **115**, 1289–1295.
- [40] S. Keller, K. Boguslawski, T. Janowski, M. Reiher and P. Pulay, *J. Chem. Phys.*, 2015, **142**, 244104.
- [41] K. Boguslawski, P. Tecmer and Ö. Legeza, *arXiv:1606.08503 [cond-mat.str-el]*, 2016, 1–15.
- [42] M. Mottet, P. Tecmer, K. Boguslawski, Ö. Legeza and M. Reiher, *Phys. Chem. Chem. Phys.*, 2014, **16**, 8872–8880.
- [43] T. Szilvási, G. Barcza and Ö. Legeza, *arXiv:1509.04241 [physics.chem-ph]*, 2015, 1–7.
- [44] K. Boguslawski and M. Reiher, in *The Chemical Bond: Chemical Bonding Across the Periodic Table*, ed. G. Frenking and S. Shaik, Wiley-VCH Verlag GmbH & Co. KGaA, 2014, ch. 8, pp. 219–252.
- [45] L. Freitag, S. Knecht, S. F. Keller, M. G. Delcey, F. Aquilante, T. B. Pedersen, R. Lindh, M. Reiher and L. Gonzalez, *Phys. Chem. Chem. Phys.*, 2015, **17**, 13769–13769.
- [46] P. Tecmer, K. Boguslawski and P. Ayers, *Phys. Chem. Chem. Phys.*, 2015, **17**, 14427–14436.
- [47] Y. Zhao, K. Boguslawski, P. Tecmer, C. Duperrouzel, G. Barcza, Ö. Legeza and P. W. Ayers, *Theor. Chem. Acc.*, 2015, **134**, 120.
- [48] V. Murg, F. Verstraete, R. Schneider, P. R. Nagy and Ö. Legeza, *J. Chem. Theory Comput.*, 2015, **11**, 1027–1036.
- [49] E. Fertitta, B. Paulus, G. Barcza and Ö. Legeza, *Phys. Rev. B*, 2014, **90**, 245129.
- [50] C. Duperrouzel, P. Tecmer, K. Boguslawski, G. Barcza, Ö. Legeza and P. W. Ayers, *Chem. Phys. Lett.*, 2015, **621**, 160–164.
- [51] P. Tecmer, K. Boguslawski, Ö. Legeza and M. Reiher, *Phys. Chem. Chem. Phys.*, 2014, **16**, 719–727.
- [52] L. Maron, T. Leininger, B. Schimmelpfennig, V. Vallet, J.-L. Heully, C. Teichteil, O. Gropen and U. Wahlgren, *Chem. Phys.*, 1999, **244**, 195–201.
- [53] I. Infante, A. S. P. Gomes and L. Visscher, *J. Chem. Phys.*, 2006, **125**, 074301.
- [54] G. L. Macchia, I. Infante, J. Raab, J. K. Gibson and L. Magliardi, *Phys. Chem. Chem. Phys.*, 2008, **48**, 7278–7283.
- [55] R. G. Denning, *J. Phys. Chem. A*, 2007, **111**, 4125–4143.
- [56] *The Chemistry of the Actinide and Transactinide Elements*, ed. L. R. Morss, N. M. Edelstein, J. Fuger and J. J. Katz, Springer, Dordrecht, The Netherlands, 4th edn., 2011.
- [57] D. Wang, W. F. van Gunsteren and Z. Chai, *Chem. Soc. Rev.*, 2012, **41**, 5836–5865.
- [58] R. G. Denning, *Struct. Bonding*, 1992, **79**, 215–276.
- [59] I. Castro-Rodriguez, H. Nakai, L. N. Zakharov, A. L. Rheingold and K. Meyer, *Science*, 2004, **305**, 1757–1759.
- [60] R. J. Baker, *Chem. Eur. J.*, 2012, **18**, 16258–16271.
- [61] A. V. Zaitsevskii, A. V. Titov, S. S. Mal'kov, I. G. Tananaev and Y. M. Kiselev, *Dokl. Chem.*, 2013, **448**, 1–3.
- [62] T. Gao, Z.-H. Zhu, X.-L. Wang, Y. Sun and D.-Q. Meng, *Acta Chim.*, 2004, **62**, 454–460.
- [63] D. Andrae, U. Häußermann, M. Dolg, H. Stoll and H. Preuß, *Theo. Chem. Acta*, 1990, **77**, 123–141.
- [64] X. Cao, M. Dolg and H. Stoll, *J. Chem. Phys.*, 2003, **118**, 487–496.
- [65] X. Cao and M. Dolg, *J. Mol. Struct. {THEOCHEM}*, 2004, **673**, 203 – 209.
- [66] T. H. Dunning, Jr., *J. Chem. Phys.*, 1989, **90**, 1007–1023.
- [67] R. A. Kendall, T. H. Dunning, Jr. and R. J. Harrison, *J. Chem. Phys.*, 1992, **96**, 6796–6806.
- [68] M. J. Frisch, G. W. Trucks, H. B. Schlegel, G. E. Scuseria, M. A. Robb, J. R. Cheeseman, J. A. Montgomery, Jr., T. Vreven, K. N. Kudin, J. C. Burant, J. M. Millam, S. S. Iyengar, J. Tomasi, V. Barone, B. Mennucci, M. Cossi, G. Scalmani, N. Rega, G. A. Petersson, H. Nakatsuji, M. Hada, M. Ehara, K. Toyota, R. Fukuda, J. Hasegawa, M. Ishida, T. Nakajima, Y. Honda, O. Kitao, H. Nakai, M. Klene, X. Li, J. E. Knox, H. P. Hratchian, J. B. Cross, V. Bakken, C. Adamo, J. Jaramillo, R. Gomperts, R. E. Stratmann, O. Yazyev, A. J. Austin, R. Cammi, C. Pomelli, J. W. Ochterski, P. Y. Ayala, K. Morokuma, G. A. Voth, P. Salvador, J. J. Dannenberg, V. G. Zakrzewski, S. Dapprich, A. D. Daniels, M. C. Strain, O. Farkas, D. K. Malick, A. D. Rabuck, K. Raghavachari, J. B. Foresman, J. V. Ortiz, Q. Cui, A. G. Baboul, S. Clifford, J. Cioslowski, B. B. Stefanov, G. Liu, A. Liashenko, P. Piskorz, I. Komaromi, R. L. Martin, D. J. Fox, T. Keith, M. A. Al-Laham, C. Y. Peng, A. Nanayakkara, M. Challacombe, P. M. W. Gill, B. Johnson, W. Chen, M. W. Wong, C. Gonzalez and J. A. Pople, *Gaussian 09, Revision C.02*, Gaussian, Inc., Wallingford, CT, 2004.
- [69] A. D. Becke, *J. Chem. Phys.*, 1993, **98**, 5648–5652.
- [70] B. O. Roos, P. R. Taylor and P. E. M. Siegbahn, *Chem. Phys.*, 1980, **48**, 157–173.
- [71] H.-J. Werner and P. J. Knowles, *J. Chem. Phys.*, 1985, **82**, 5053–5063.
- [72] H.-J. Werner, P. J. Knowles, R. Lindh, F. R. Manby, P. C. M. Schütz, T. Korona, A. Mitrushenkov, G. Rauhut, T. B. Adler, R. D. Amos, A. Bernhardsson, A. Berning, D. L. Cooper, M. J. O. Deegan, A. J. Dobbyn, F. Eckert, E. Goll, C. Hampel, G. Hetzer, T. Hrenar, G. Knizia, C. Köppl, Y. Liu, A. W. Lloyd, R. A. Mata, A. J. May, S. J. McNicholas, W. Meyer, M. E. Mura, A. Nicklass, P. Palmieri, K. Pflüger, R. Pitzer, M. Reiher, U. Schumann, H. Stoll, A. J. Stone, R. Tarroni, T. Thorsteinsson, M. Wang and A. Wolf, *MOLPRO, Version 2012.1, A Package Of Ab Initio Programs*, 2012, see <http://www.molpro.net>.
- [73] H.-J. Werner, P. J. Knowles, G. Knizia, F. R. Manby and M. Schütz, *WIREs Comput. Mol. Sci.*, 2012, **2**, 242–253.
- [74] Jmol: An Open-Source Java Viewer for Chemical Structures in 3D. <http://www.jmol.org/>.
- [75] Ö. Legeza, QC-DMRG-BUDAPEST, *A Program for Quantum Chemical DMRG Calculations*. Copyright 2000–2016, HAS RISSPO Budapest.
- [76] Ö. Legeza, J. Röder and B. A. Hess, *Phys. Rev. B*, 2003, **67**, 125114.
- [77] Ö. Legeza and J. Sólyom, *Phys. Rev. B*, 2004, **70**, 205118.
- [78] Ö. Legeza and J. Sólyom, *Phys. Rev. Lett.*, 2006, **96**, 4–7.
- [79] C. J. Stein and M. Reiher, *J. Chem. Theory Comput.*, 2016, **12**, 1760–1771.
- [80] S. Szalay, G. Barcza, T. Szilvási, L. Veis and Ö. Legeza, *arXiv:1605.06919 [quant-ph]*, 2016, 1–10.